



# Experimental Investigations on Hydro-mechanical Processes in Reconstituted Clay Shale and Their Significance for Constitutive Modelling

Antonia Nitsch<sup>1,2</sup> · Julia Leuthold<sup>3</sup> · Jan Machaček<sup>1,4</sup> · Carlos Eduardo Grandas Tavera<sup>2</sup>

Received: 19 April 2022 / Accepted: 12 December 2022 / Published online: 11 January 2023  
© The Author(s) 2023

## Abstract

The hydro-mechanical processes of a reconstituted clay shale (Opalinus Clay) were studied and implications for constitutive modelling of swellable clay shales derived. The study aims to provide further insights into these coupled processes. For that, oedometric swelling tests with varying boundary conditions and loading paths, oedometric compression tests under dry and saturated conditions, and permeability tests were performed. The results showed a unique preloading line for the dry state when plotting the void ratio against the vertical stress. For saturated states, this line was shifted to the left (to smaller stresses) which revealed a severe reduction of preloading stress due to saturation. All loading paths converged in a normal compression line (NCL) regardless of the mechanical boundary conditions during saturation. A trend line affine to the NCL was established for swelling pressures at different initial void ratios. The influence of saturation on the mechanical properties became further evident, as the un-/reloading stiffness was significantly reduced. A linear relationship between volumetric deformation and saturation was found. A severe swelling induced reduction of permeability in the saturated state was demonstrated and confirmed by the analysis of consolidation processes during oedometric loading. The experimental findings were used to derive fundamental assumptions for constitutive modelling and were discussed within a numerical framework for expansive soils.

## Highlights

- Oedometric swelling and compression tests considering different hydro-mechanical loading paths were conducted to evaluate the swelling induced changes of the mechanical properties.
- Experimental results show reductions of both preloading stress and elastic stiffness due to saturation. Long monotonic loading leads to a unique normal compression line (NCL).
- A linear coupling between swelling deformation and saturation was found by testing in perspex oedometer rings.
- Permeability measurements in the dry and saturated state establish a swelling-induced reduction in permeability.

---

✉ Antonia Nitsch  
antonia.nitsch@rub.de

Julia Leuthold  
julia.leuthold@kit.edu

Jan Machaček  
jan.machacek@tu-darmstadt.de

Carlos Eduardo Grandas Tavera  
carlos.grandastavera@b-tu.de

<sup>2</sup> Department of Architecture, Civil Engineering and Urban Planning, Chair of Soil Mechanics and Foundations/Geotechnical Engineering, Brandenburgische Technische Universität Cottbus-Senftenberg, Cottbus, Germany

<sup>3</sup> Institute of Soil Mechanics and Rock Mechanics, Karlsruher Institut für Technologie, Karlsruhe, Germany

<sup>4</sup> Department of Civil and Environmental Engineering, Institute of Geotechnics, Technische Universität Darmstadt, Darmstadt, Germany

<sup>1</sup> Present Address: Department of Civil and Environmental Engineering, Chair of Soil Mechanics, Foundation Engineering and Environmental Geotechnics, Ruhr Universität Bochum, Bochum, Germany

- The results are discussed within a framework of constitutive modelling of expansive soils.

**Keywords** Hydro-mechanical behaviour · Swelling · Oedometric compression · Permeability · Constitutive modelling

## 1 Introduction

The hydro-mechanical behavior of shales is of particular interest for various applications in geomechanics. Due to their low permeability and their high sorption ability, shales are considered as potential host rocks for nuclear waste disposal (Nagra 2014; Marschall et al. 2005) and as a cap rock material for CO<sub>2</sub> capture and storage in deep geological layers (Chevalier et al. 2010). In these applications, the shale is subjected to changes in the stress state which leads to alterations in porosity, permeability and stiffness. Furthermore, the clay shales are overconsolidated and experience swelling phenomena, imposing high demands on the assessment of the hydro-mechanical response of the material.

The material behavior of shales in the intact, remoulded or reconstituted state under hydro-mechanical loading has been studied in the past few decades. Fundamental experimental investigations focused either on the compression or the swelling behavior and have been conducted on different shales such as Callovo-Oxfordian Clay shale (Zhang and Rothfuchs 2004; Tang et al. 2010), Queenston shale (Lo and Lee 2011), Pierre shale (Savage and Braddock 1991) or La Biche shale (Wong 1998). Studies about the coupled behavior of overconsolidated clay shales combining mechanical and hydraulic loading paths have become more of a focus of current research in recent years. In a study by Mohajerani et al. (2011) the hydro-mechanical properties of Callovo-Oxfordian Claystone were investigated by means of oedometric compression tests where the swelling deformation process was also considered. Besides, Vergara (2019) documented a significant strength and stiffness reduction in overconsolidated clay shales after swelling. The majority of testing was carried out on intact samples, but the material behavior of remoulded and reconstituted clay shale has been increasingly studied recently, as mixtures of clay shale and bentonites are being investigated as a possible buffer material in the context of deep geological storage (Zeng et al. 2021; Zhang and Kröhn 2019; Souza and Pejon 2020). For a characterisation of clay shales for in situ application, testing on intact specimens is essential, since processes that arise from the natural formation of the shale and diagenesis are hardly considered otherwise. However, William and Airey (2009) showed in their study on Bringelly shale that depending on the degree of cementation of a shale, it can also be sufficient to compact the remoulded material to the same void ratio like the intact material since the differences in stiffness are negligible. For other shales, the impact of

diagenesis on the hydro-mechanical behavior were found to be more significant, e.g., for Kimmeridge Clay shale (Nygård et al. 2004) and also Opalinus Clay shale (Favero et al. 2016). In the investigations of Crisci et al. (2019) and Favero et al. (2016), it was shown that in the saturated state the remoulded material has a greater compressibility than the intact shale, which is reflected by significantly higher compression and swelling indices. With the results, a mechanism of porosity reduction due to mechanical compaction and diagenesis was derived by Favero et al. (2016), which allows an evaluation to which extent testing on remoulded material is sufficient to obtain information of the intact material. However, for the experimental investigation of basic physical processes during saturation and hydro-mechanical loading uniform samples are preferred and in this context the usage of reconstituted samples can provide valuable results (Crisci et al. 2019; Seiphoori et al. 2016; Zeng et al. 2021).

For Opalinus Clay shale an extensive study on the fundamental relationships between different hydro-mechanical parameters including a variation of boundary conditions during saturation is still missing. Ferrari et al. (2016) studied the compression and consolidation behavior of intact Opalinus Clay shale presenting an analytical approach to derive fundamental hydro-mechanical properties such as the coefficient of consolidation, stiffness and permeability of the tested material as a function of the applied stress conditions. Experimental results of oedometric compression tests and constant-head permeability tests on saturated intact and remoulded material have been reported by Crisci et al. (2019). It was shown that the material state has a more significant effect on the mechanical behavior than on the permeability. An expected decrease in hydraulic conductivity in the saturated state for decreasing void ratios in steady-state permeability testing became evident, yielding hydraulic conductivities in the range of  $k = 10^{-12} - 10^{-14}$  m/s. Similar values were reported by Winhausen et al. (2021). However, only the permeability in the saturated state is provided and an evaluation of the swelling induced reduction of permeability is missing. Similar investigations by Favero et al. (2016) compared the hydro-mechanical properties of intact and remoulded samples of Opalinus Clay shale during compression. A detailed comparison of the micro structure and its influence on the hydro-mechanically coupled material behavior has been provided by Seiphoori et al. (2016, 2017).

All of these studies investigated different aspects of the hydro-mechanical response under different boundary conditions, but the interaction between the different processes was

not fully examined. To the authors' knowledge, the influence of the mechanical boundary conditions during the saturation of the material on the behavior under subsequent oedometric loading has not been investigated. Furthermore, the effect of the mechanical loading history on the swelling behavior is rarely considered. The aim of this study is to fill this gap by investigating different physical processes occurring during hydro-mechanical loading of reconstituted clay shale. The focus is to investigate the swelling behavior in interaction with the mechanical behavior and, based on this, to derive relations and fundamental assumptions for the constitutive description of such a material. The material response in different swelling tests, oedometric compression tests and permeability tests is studied with regard to the coupling between saturation, swelling behavior and mechanical loading history. The identification of individual processes and their contribution to the overall material behavior enables the phenomenological derivation of fundamental principles for the continuum mechanical description of the material.

Parallel to the experimental investigation of swellable and expansive soils, a wide range of models and methods have been developed to describe the observed hydro-mechanical coupled material behaviour. It is beyond the scope of this paper to provide a complete overview of the multitude of analytical and numerical approaches, but some concepts are briefly introduced. One of the first formulations was provided by Grob (1972), correlating maximum strains with stresses that can be reached during wetting. Emerging from the field of rock mechanics and tunnelling this basic swelling law and its extensions considering, e.g., time effects and anisotropy (Heidkamp 2004; Anagnostou 1993; Kiehl 1990; Wittke-Gattermann and Wittke 2004) are suitable for unloading processes, but do not include a coupled description of the material behavior. More sophisticated constitutive models for unsaturated and expansive soils were introduced, led by the Barcelona Basic Model (BBM) of Alonso et al. (1990). Therein, the suction is used to account for the material behavior in the unsaturated state, either used as an internal variable for hardening or directly as a second stress domain in addition to either the net stress, cf. Alonso et al. 1990, 1999; Gens and Alonso 1992 and Cui and Delage 1996) amongst others, or effective stress (Zhou et al. 2012; Bosch et al. 2021; Mašín and Khalili 2008). When incorporating expansive behavior, most models use a double-porosity approach as first introduced in the Barcelona Expansive Model (BExM) (Gens and Alonso 1992; Alonso et al. 1999) with an expansion of the microstructure. Although introducing micro- and macrostructure provides a suitable modelling framework, the determination of state variables and model parameters from different structure levels is challenging and does not generally apply to all materials such as clay shales, which tend to have a mono-modal pore distribution (Seiphoori et al. 2016; Mohajerani et al. 2011).

Instead of suction, the (effective) degree of saturation can be used, as shown, e.g., by Zhou et al. (2012). The (effective) degree of saturation and its relation to the suction is given by the soil water retention curve. Simple models, e.g., after van Genuchten (1980), or more sophisticated approaches for expansive soils such as developed by Dieudonne et al. (2017) and Della Vecchia et al. (2015) can be used. Introducing the (effective) degree of saturation as a driving variable in a constitutive model offers two very attractive advantages: (1) the transition between unsaturated and saturated states occurs naturally and (2) evolution equations and other mathematical expressions are simplified due to its range between 0 – 1. Therefore the authors of this work, Grandas Tavera et al. (2022), developed a novel constitutive model formulated in net stress and (effective) degree of saturation, which is phenomenologically based on the experimental results presented in this manuscript amongst other studies. The description of the model exceeds the scope of this paper, but details can be found in Grandas Tavera et al. (2022). In this work, the interpretation of the experimental results regarding the constitutive description of a swellable soil is presented.

The paper is structured as follows. First, the material and the sample preparation are presented in Sect. 2. Following, the testing equipment, test methods and experimental programme are explained in Sect. 3. The test results are presented and then analysed with regard to the dependencies of the results on different test methods in Sect. 4. Here, the results are compared with the results of other experimental studies. In the course of this, a relation of the individual processes as the basis for a continuum-mechanical description of the material behavior is presented. A detailed discussion of the experimental results in regard to their implications for constitutive modelling is provided in Sect. 5. The work concludes with a summary of the observed phenomena in Sect. 6.

## 2 Materials and Specimen Preparation

### 2.1 Tested Material

The material used in this study is Opalinus Clay Shale from the clayey facies in the Mont Terri Underground Rock Laboratory (URL) in Switzerland ( $\rho_s = 2.718 \text{ g/cm}^3$ ). The location of the blocks is not known so that no information about the sampling depth can be given. Opalinus Clay Shale is a fine-grained sedimentary rock that was deposited approximately 180 million years ago during the Aalenian stage of the Middle Jurassic. Subsequently, it was subjected to several burial stages with overburdening heights between 1000-1350 m due to the lowering of the Rhine Graben. In the further course of its formation it experienced uplift and tilting during the Alpine orogeny (Bossart 2012; Mazurek

et al. 2006; Wetzel and Allia 2003). Nowadays, the maximum 200 m thick layers of the clayey facies of Opalinus Clay Shale is found at a depth of about 300 m and is therefore considered as overconsolidated Nagra (2005). The mineralogical composition of the studied shale was determined in a x-ray-diffraction analysis and is reported in Table 1. The clay content is 56 % mass in total, which is in good agreement with the characteristics for Opalinus clay shale from Mont Terri reported by Bossart (2012).

In this study all experiments were carried out on reconstituted specimens. In order to attain repeatability of the experiments, a large number of tests on specimens with a small scattering in the material properties was produced. Another reason for the usage of reconstituted samples was to control the loading history of the samples to investigate the influence of mechanical preloading on the material behavior.

## 2.2 Specimen Preparation

A procedure has been developed to prepare reconstituted specimens. In a first step, a powder from the intact rock material was produced. Therefore, irregular formed hand pieces of the material were cut with a saw into smaller blocks and crushed with a jaw crusher. The material was then ground to a fine powder with a laboratory mortar grinder. The powder was not further processed or sieved, so that the mineralogical composition of the intact rock was preserved.

A hydrometer analysis of two batches has been conducted afterwards as is shown in Fig. 1. The residual water content of the powder is  $w = 1.82\%$ .

Specimens were prepared by compressing the powder in an oedometer ring up to the desired dry density  $\rho_d$ . This was realized by specifying the mass and the target height of the specimens. The required high pressures were applied by a servo-controlled uniaxial test setup, see Fig. 2a. A special preparation apparatus was mounted into the loading frame, see Fig. 2b and c. At the beginning of the preparation the powdered material was poured in a thick-walled steel hollow cylinder with the respective oedometer ring positioned at the bottom. The oedometer rings have an inner diameter of 60 mm, an outer diameter of 70 mm and a height of 20 mm. The loading piston was placed loosely on top of the material and the loading plate is lowered with a constant strain rate of  $\dot{s} = 0.5$  mm/min until finally the piston was fully immersed in the cylinder and the loading plate was in contact with the upper surface of the cylinder. In this way, the compacted specimen is always level with the top of the oedometer ring and the sample height can be controlled by the use of specific spacers. Then the loading plate was fixed and the specimen was compacted for 30 minutes. The axial load was measured by an external load cell below the bottom loading

**Table 1** Mineralogical composition of the tested Opalinus clay shale (% mass)

Smectite	5
Illite	32
Chlorite	9
Kaolinite	10
Quarz	8
Feldspars-Ka	2
Feldspars-Na	2
Calcite	6
Dolomite	<0,1
Ankerite	<1,5
Siderite	1
Pyrite	<1,5
Apatite	1
Amorphous	≈ 20

plate. Afterwards the samples were removed from the test setup, measured, weighed and stored in a protected environment. A compacted sample inside an oedometer ring is shown in Fig. 3. During preparation of the reconstituted specimen it became evident, that the very little void ratios of intact Opalinus Clay shale could not be reached only by static compaction, as is also reported by, e.g., Crisci et al. (2019).

To investigate the effect of the preparation method on the mechanical behavior, different methods like pluviation and layer-wise tamping have been tested. The experimental results showed no influence on the mechanical behavior and hence, pluviation was used in the specimen preparation. In Fig. 4a the temporal progression of the total axial

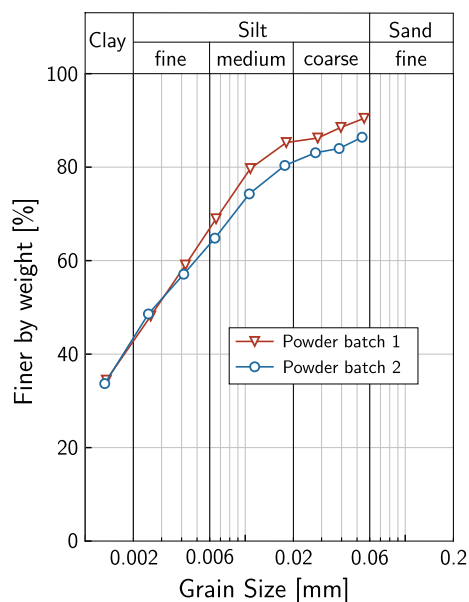


**Fig. 1** Grain size distribution curve of powdered Opalinus Clay shale

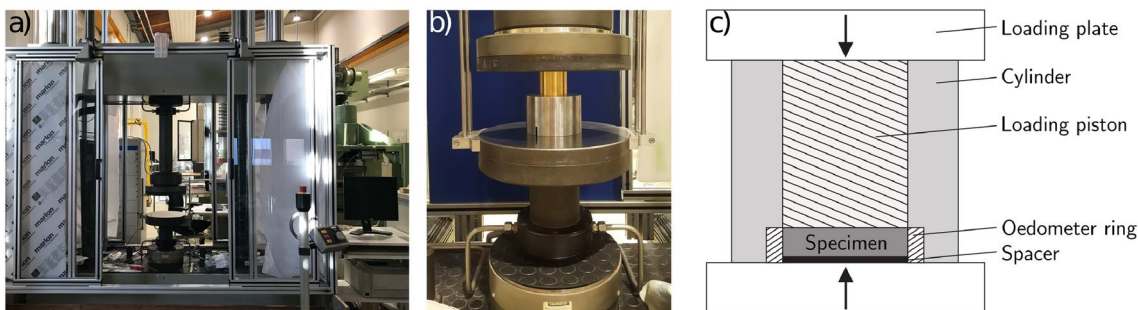


Fig. 2 Experimental setup for specimen preparation: a Servo-controlled loading frame. b and c Preparation apparatus

stress  $\sigma$  during the preparation procedure is shown. A unique relation between the target dry density  $\rho_d$  (or void ratio  $e = \rho_s / \rho_d - 1$ ) and the required stress can be identified with a slope of the first compression line of  $C_C = 0.208$  (compression index), see Fig. 4b. Moreover, it is possible to approximate the unloading index of  $C_S = 0.021$  (swelling index) by the measurements of the height of the compacted samples inside the oedometer ring after the preparation (faint lines). The indices were determined as follows:

$$C_S = - \frac{\Delta e}{\log_{10} \left( \frac{\sigma_v}{\sigma_0} \right)} \quad \text{and} \quad C_C = \frac{\Delta e}{\log_{10} \left( \frac{\sigma_v}{\sigma_e} \right)}, \quad (1)$$

with  $\sigma_0$  and  $\sigma_e$  being the stresses on the first compression and unloading line corresponding the void ratio change  $\Delta e$ .

The required stress for compaction is shown with markers in Fig. 4b. As the loading plate was in contact with the hollow cylinder, any additional stress did not act on the sample, but on the preparation apparatus instead. A stress relaxation during compaction becomes evident, see Fig. 4a. Table 2 summarizes the preparation characteristics of the tests as well as the initial water content  $w$  and degree of saturation  $S$ . Having a unique compression

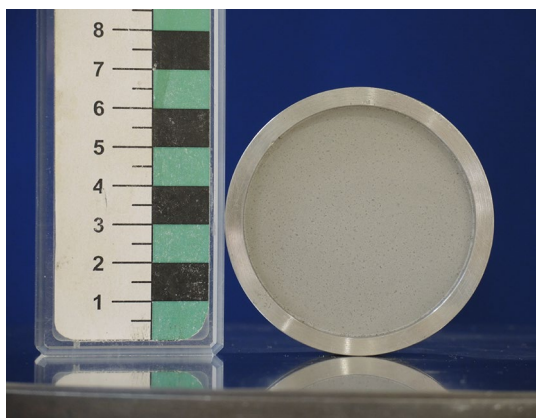


Fig. 3 Specimen inside oedometer ring after compaction

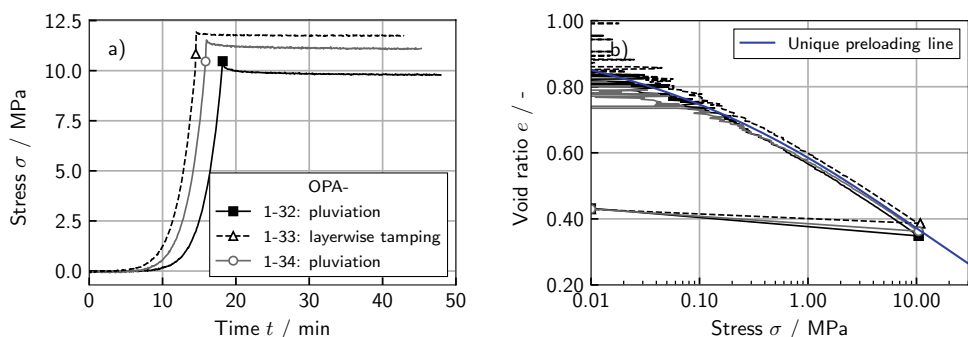
Table 2 Summary of the preparation characteristics of three representative tests

Specimen OPA-	Initial conditions after compaction			Preloading stress [MPa] <sup>1</sup>
	$e$ [-]	$\rho_d$ [g/cm <sup>3</sup> ]	$S$ [-]	
1-32	0.432	1.899	0.126	10.74 (9.85)
1-33	0.429	1.902	0.127	10.84 (10.38)
1-34	0.430	1.901	0.126	10.46 (10.25)

\* The initial water content of all specimens was  $w = 1.82\%$

<sup>1</sup> Values shown within brackets correspond to the stress after relaxation

Fig. 4 Specimen preparation: a Stress vs. time during compaction. b Void ratio vs. stress during compaction. Note that the oscillations are due to the resolution of the load cell in the range of small stresses



line during preloading, the preconsolidation stress for any dry density of the specimens can be approximated. Most specimens in this study have a target dry density of  $\rho_{d,0} = 1.930 \pm 0.03 \text{ g/cm}^3$ , which corresponds to a preparation stress of  $\sigma_{\text{prep}} = 10 - 11 \text{ MPa}$ . The preloading stress  $\sigma_{\text{prep}}$  of the specimens was only varied in the oedometric swelling tests to investigate the influence of preloading on the swelling behavior.

### 3 Testing Equipment and Test Methods

The study includes oedometric swelling tests, oedometric compression tests and permeability measurements. Test setups and test methods used in this study are presented in the following.

The oedometric swelling tests and oedometric compression tests are carried out in an open watering cell (Fig. 5), which was mounted in three different loading frames for specific loading paths. The specimen inside the oedometer ring can easily be installed between a lower and upper porous stone. The bottom of the cell and the loading piston have special cutouts to secure a steady and continuous water supply through the porous stones to the sample. The watering cell allows water supply to the sample from the bottom and the top by filling the watering cell to the desired height.

The majority of the tests are performed in a standard oedometric swelling cell, further referred to as *test setup 1*. The test setup was developed at the Institute of Soil Mechanics and Rock Mechanics (IBF) at the Karlsruhe Institute of Technology (KIT) and last modified by Vergara (2019). A detailed description and comparison to other simple cells can be found in Vergara et al. (2014). The test setup is shown in Fig. 6. The watering cell is mounted in a simple loading frame with a manually controlled load spindle on top of the specimen and a load cell located at the bottom of the cell. The vertical

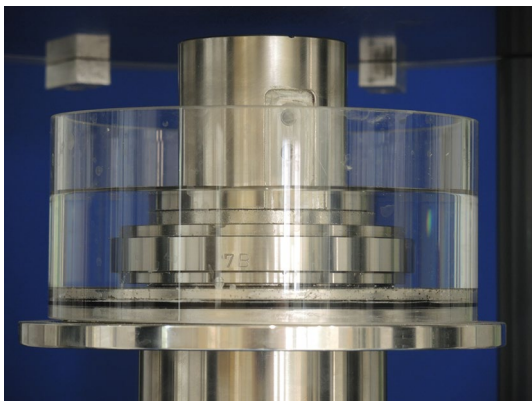


**Fig. 5** Specimen inside oedometer ring after compaction in open watering cell

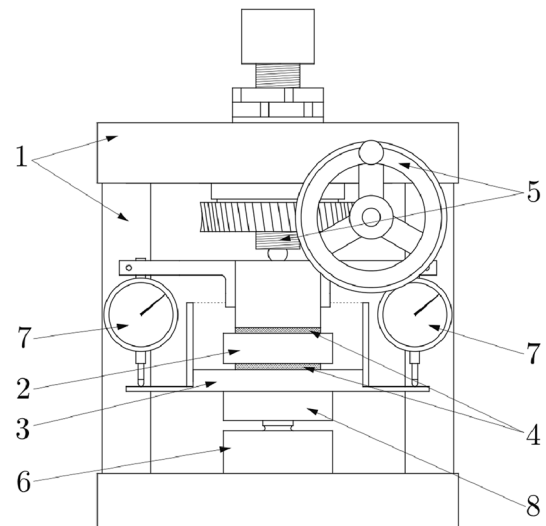


**Fig. 6** Test setup 1 for oedometric swelling tests. Schematic drawing: (1) rigid frame, (2) oedometric ring with specimen, (3) watering cell, (4) porous metal plates, (5) spindle, (6) load cell and (7) dial gauges and (8) steel plate. Modified from Vergara (2019)

deformation is measured by two gauges with an accuracy of 0.001 mm at opposite sides of the specimen. To perform a test under constant volume and constant stress conditions the vertical deformation has to be corrected manually.

To improve the precision of the test control and apply larger stresses during oedometric compression tests, two servo-controlled test setups were used. In *test setup 2* the open watering cell is mounted in the servo-controlled loading frame used for specimen preparation (see Sect. 2.2, Fig. 2). As the acquisition system of the machine itself is outdated, the axial strain and the axial stress are measured with an external acquisition system, see Fig. 7. The axial displacement is measured with three displacement transducers against an aluminium ring that is fixed to the axial piston of the machine. The axial stress is measured with a load cell with a load capacity of 900 kN under the open watering cell. For *test setup 3* a servo-controlled test machine type 815 from the company MTS is used. Similar to test setup 2 the open watering cell is installed in the loading frame and the axial stress is measured with a load cell with a load capacity of 250 kN under the open watering cell. The vertical displacement is measured by the axial displacement of the loading piston. A more detailed description of the machine itself is given in Leuthold et al. (2021). This test setup is the best facility to get accurate results at small axial loads and with complex loading paths and was therefore, used for the long lasting oedometric compression tests after swelling.

The permeability testing is performed in *test setup 4*, which consists of the same simple loading frame used in *test setup 1*, but is modified by the usage of a fluid-tight pressure cell instead of an open watering cell. The axial deformation is measured with one strain gauge with an accuracy of 0.001 mm between

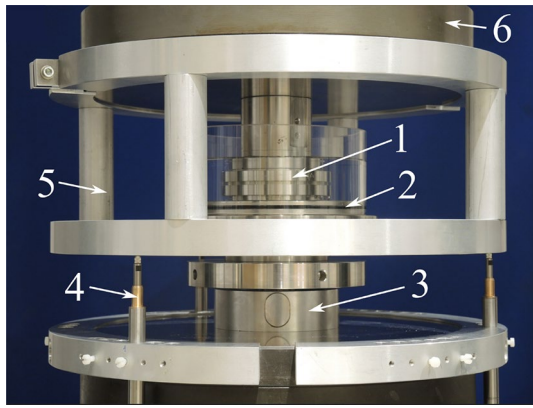


**Fig. 7** Test setup 2 for oedometric swelling tests and oedometric compression tests: (1) oedometric ring with rock specimen, (2) watering cell, (3) load cell, (4) displacement transducers, (5) aluminium ring and (6) loading piston

the loading plate and the bottom of the watering cell. The axial stress is measured with a load cell located at the bottom. For water permeability testing the pressure cell is connected to an upstream and downstream stand pipe, in which the volume of water flowing through the sample in a certain time interval can be determined (see Fig. 8b). Pressure difference in the water is achieved using air pressure. A more detailed description is provided in Vergara (2019). For air permeability testing the pressure vessel is connected to a gas supply at the bottom and a soap bubble flow meter at the top drainage (see Fig. 8c). The volume of gas flow through the sample is evaluated by measuring the time of the outflowing gas passing a defined volume in the soap covered bubble flow meter.

### 3.1 Oedometric Swelling Tests

The material’s ability to swell has a significant effect on the hydro-mechanical behavior. To distinguish the different physical processes during saturation depending on the hydro-mechanical boundary conditions and to ensure reproducibility of the results, 30 oedometric swelling test were performed (see Table 3). The results of all tests are used in the analysis of this work, but for the sake of clarity, detailed discussion is limited to 12 representative tests only. The initial dry density was varied between  $\rho_d = 1.693 - 2.013 \text{ g/cm}^3$ . Most of the swelling tests were carried out in *test setup 1*. To investigate the effect of the manual adjustment of the axial displacement on the swelling process, swelling pressure tests were also performed in *test setup 2*. The experimental results showed that the manual control of the axial displacement has no effect on the swelling behavior so that all further swelling tests were performed in *test setup 1*. Except one, all swelling tests in this study were performed with water supply from the top and the bottom.

Within this study swelling tests with different stress-strain paths have been investigated which are shown in Fig. 9 and as well summarized in Table 3. In addition to single-step swelling pressure tests (confined conditions, Fig. 9, A-B) and single-step swelling strain tests (unconfined conditions, Fig. 9, A–D) a variety of multi-step tests has been carried out. The aim was to investigate the effect of the loading sequence on the axial deformation. Therefore, some specimens were unloaded from their swelling pressure (Fig. 9, B) to half of the swelling pressure (Fig. 9, C) and to the initial fixing stress (Fig. 9, D) (stress-controlled). Additionally, the loading sequence was carried out in reverse direction: the

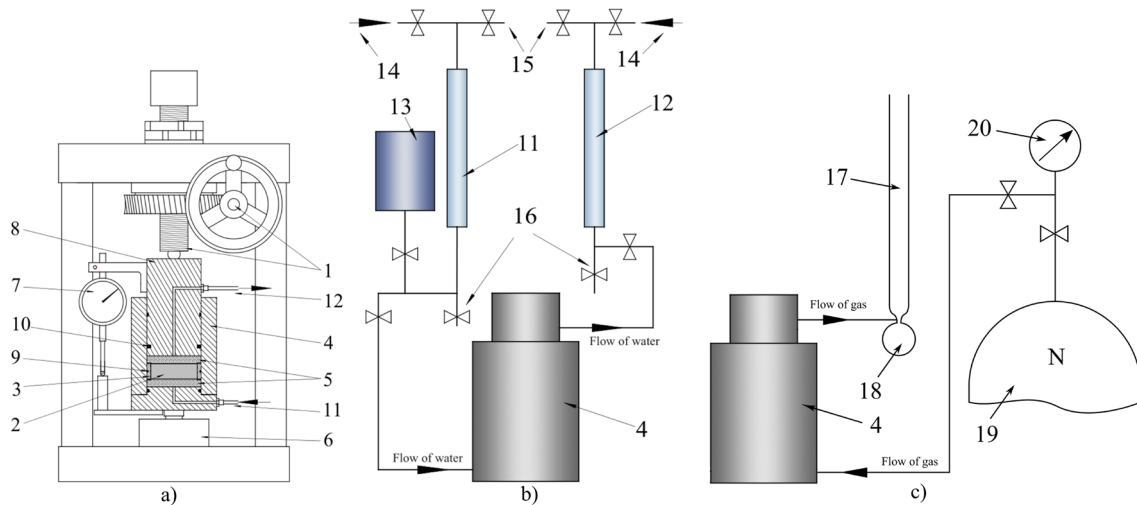


**Fig. 8** Test setup 4 for permeability testing. Schematic drawing of a) Swelling test apparatus b) Pressure cell and stand pipe system for water permeability testing and c) Soap bubble flow meter for air permeability testing. (1) manual spindle, (2) specimen, (3) oedometer ring, (4) pressure vessel, (5) porous discs, (6) load cell, (7) dial

gauge, (8) loading piston, (9) O-ring, (10) piston seal, (11) upstream graduated stand pipe, (12) downstream graduated stand pipe, (13) water supply, (14) air pressure/vacuum, (15) air bleed, (16) water outlet, (17) flow meter, (18) soap bubble, (19) nitrogen reservoir and (20) pressure gauge. Modified from Vergara (2019)

**Table 3** Summary of the performed oedometric swelling tests, sorted by loading paths and initial conditions

Specimen OPA-	Path <sup>a</sup>	Initial conditions *		
		$e$ [-]	$\rho_d$ [g/cm <sup>3</sup> ]	$S$ [-]
1-21	A-B	0.576	1.725	0.086
1-22	A-B	0.564	1.738	0.088
1-09	A-B	0.564	1.739	0.088
1-01	A-B	0.434	1.896	0.114
1-03	A-B	0.387	1.960	0.128
1-12	A-B	0.386	1.962	0.128
1-02	A-B	0.351	2.013	0.141
1-07	A-B-C	0.602	1.697	0.082
0-03	A-B-C	0.393	1.952	0.126
1-04	A-B-C	0.386	1.962	0.128
1-05	A-B-C	0.385	1.963	0.128
0-05	A-B-C	0.379	1.972	0.130
1-08	A-B-C-D	0.606	1.693	0.082
1-10	A-B-C-D	0.564	1.739	0.088
0-07	A-B-C-D	0.392	1.953	0.126
0-06	A-B-C-D	0.388	1.959	0.127
1-06	A-B-C-D	0.386	1.961	0.128
0-04	A-B-C-D	0.385	1.963	0.128
1-11	A-B-C-D <sup>2</sup>	0.384	1.964	0.129
0-02	A-B-C-D	0.382	1.967	0.129
0-29	A-B-C'-C'' <sup>3</sup>	0.382	1.968	0.129
1-17	A-D	0.419	1.916	0.118
0-24	A-D	0.386	1.962	0.128
0-32	A-D	0.377	1.975	0.131
1-15	A-D-C <sup>4</sup>	0.386	1.962	0.128
1-16	A-D-C-B	0.386	1.962	0.128
0-15	A-D <sup>P</sup>	0.388	1.959	0.127
0-14	A-B <sup>P</sup>	0.380	1.970	0.130
1-30	A-D <sup>6</sup>	0.385	1.963	0.128
1-31	A-D <sup>6**</sup>	0.383	1.965	0.129

\* The initial water content of all specimens was  $w = 1.82\%$

<sup>a</sup> See Fig. 9

<sup>1</sup> In test setup 2

<sup>2</sup> Unloading to  $\sigma = 0.75 \cdot \sigma_{\max}$

<sup>3</sup> Unloading to  $e \approx 0.20 \cdot e_{\max}$  and  $e \approx 0.45 \cdot e_{\max}$

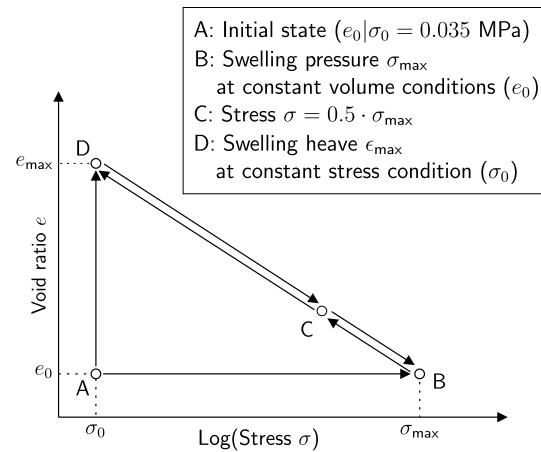
<sup>4</sup> Loaded to an estimated stress of  $\sigma \approx 0.45 \cdot \sigma_{\max}$  and  $\sigma \approx 0.90 \cdot \sigma_{\max}$

<sup>P</sup> Testing in perspex ring

<sup>6</sup> Test stopped after 5 minutes

\*\* Watering only from the bottom

specimens were loaded after unconfined swelling (Fig. 9, D) to the estimated half of the swelling pressure (Fig. 9, C) and estimated swelling pressure (Fig. 9, B). In this context possible effects of the control variable were also studied by unloading one sample not to a specific stress but estimated strain (strain-controlled, referred to as A-B-C'-C'').

**Fig. 9** Test paths of the oedometric swelling tests

To investigate the relation between the degree of saturation and the swelling process, one single-step swelling strain test and one single-step swelling pressure test were performed in perspex oedometer rings in *test setup 1*. The specimens were prepared as explained in Sect. 2.2. Afterwards they were pressed out of the steel oedometer ring and subsequently pressed in the perspex ring and the height of the specimens was measured. The subsequent pressing led to a small increase in density. In order to observe the propagation of the wetting front in the specimen through the ring, the water was only supplied to the sample from the bottom in these tests. A camera was permanently installed in front of the test setup to record the progress of the wetting front in the specimen. The tests were stopped when the peak swelling pressure  $\sigma_{\max, \text{peak}}$  and the peak swelling strain  $e_{\max}$  was reached or when the water front had reached the top of the specimen. The degree of saturation at the end of the test was determined by oven-drying at  $105^\circ\text{C}$ . To gain further insight into the direct coupling of saturation and deformation two short single-step swelling strain tests (5 minutes) were performed. One specimen was watered from both sides while the second specimen was only watered from the bottom.

### 3.2 Oedometric Compression Tests Before and After Swelling Tests

To investigate the mechanical behavior of the material before and after swelling, oedometric compression tests were performed on samples before and after saturation, respectively. The oedometric compression tests before saturation are performed in *test-set up 2*. The sample inside the oedometer ring is set in the open watering cell without supplying water (atmospheric conditions) and the axial stress is applied with an axial piston with a diameter of 60 mm on the specimen. The tests are strain controlled and performed with an axial strain rate of  $\dot{s} = 0.1 \text{ mm/min}$ . As the material is nearly dry the consolidation is not considered.



For the oedometric compression tests after saturation *test setup 3* is used. To clarify whether the swelling process affects the preloading stress and the stiffness, oedometric compression tests under drained conditions are performed on saturated samples, which experienced different stress paths during swelling. In total three oedometric compression tests on saturated material have been performed:

1. After swelling under confined conditions (single-step swelling pressure test, OPA-0-34)
2. After swelling under unconfined conditions ( $\sigma \approx 0$ , single-step swelling strain test, OPA-0-24)
3. After a multi-step test (swelling pressure test with subsequent unloading, OPA-0-07).

For efficiency reasons the prior single-step swelling strain tests and multi-step test are performed in the standard cell (*test setup 1*) and afterwards transferred to *test setup 3*. It is

**Table 4** Summary of the performed oedometric compression tests before and after saturation

Specimen OPA-	Path <sup>a</sup>	Initial conditions*		
		$e$ [-]	$\rho_d$ [g/cm <sup>3</sup> ]	$S$ [-]
1-34	Dry	0.397	1.946	0.124
0-33	Dry	0.376	1.977	0.131
0-28	Dry	0.382	1.967	0.129
0-34	A-B	0.393/0.393 <sup>1</sup>	1.953/1.953 <sup>1</sup>	0.126/1.00 <sup>1</sup>
0-24	A-D	0.386/0.510 <sup>1</sup>	1.962/1.797 <sup>1</sup>	0.128/1.00 <sup>1</sup>
0-07	A-B-C-D	0.392/0.464 <sup>1</sup>	1.953/1.857 <sup>1</sup>	0.126/1.00 <sup>1</sup>

\* The initial water content of all specimens was  $w = 1.82\%$

<sup>a</sup> See Fig. 9

<sup>1</sup> Values correspond to the start of the oedometric compression test (saturated state,  $S = 1.0$  is assumed)

assumed that only a minimal elastic deformation is generated by the de- and reinstallation, so that it is not further considered. In contrast to the oedometric compression tests under dry conditions the axial stress is not applied continuously, but in steps. To guarantee drained conditions and assure consolidation during the loading steps, a preliminary consolidation test is performed on a saturated specimen. A duration of 12 hours for the initial loading and four hours for the un- and reloading paths has been established.

All oedometric compression tests include unloading and reloading cycles. An overview of the oedometric compression tests is given in Table 4.

### 3.3 Permeability Testing

The permeability  $K$  of the material might be affected by the swelling process depending on the current boundary conditions. Therefore, the permeability is measured before saturation on the nearly dry material and during different stages of oedometric swelling tests. Testing before saturation is done with steady state air-permeability testing in *test setup 4b* on six samples.

The permeability of saturated samples is measured with steady state water-permeability testing during two swelling tests in *test setup 4a*. The stress paths during the swelling process are chosen identically to those from oedometric compression tests. One swelling test is performed as a multi-step test consisting of a volume constant step and a complete unloading to the initial stress  $\sigma_0$  in the second step (9, A–B–D). The second swelling test is a single-step swelling strain test (9, A–D). At the end of each step, when the swelling pressure or the axial strain respectively reaches equilibrium, a water flow with a set pressure is applied from the bottom drainage. After the flow reached a steady-state the flow rate and thus, the permeability, are determined. The applied pressure is varied to investigate its effect on the water flow. A summary of the samples used for permeability testing is shown in Table 5.

**Table 5** Summary of the performed permeability tests

Specimen OPA-	Path <sup>a</sup>	Pressure [kPa]	Initial conditions*		
			$e$ [-]	$\rho_d$ [g/cm <sup>3</sup> ]	$S$ [-]
0-08	Dry	25, 50, 70	0.388	1.959	0.127
0-09	Dry		0.388	1.959	0.127
0-10	Dry		0.391	1.955	0.126
0-11	Dry		0.391	1.955	0.126
0-12	Dry		0.385	1.963	0.128
0-13	Dry	0.389	1.958	0.127	
0-22	A-B-D	100, 200, 400	0.387 <sup>1</sup> / 0.460 <sup>2</sup>	1.960 <sup>1</sup> / 1.862 <sup>2</sup>	0.128/1.0 <sup>2</sup>
0-35	A-D		0.387/ 0.502 <sup>2</sup>	1.961/1.810 <sup>2</sup>	0.128/1.0 <sup>2</sup>

\* The initial water content of all specimens was  $w = 1.82\%$

<sup>a</sup> See Fig. 9

<sup>1</sup> Values correspond to the start of the steady-state water flow at  $e = 0$  (saturated state,  $S = 1.0$  is assumed)

<sup>2</sup> Values correspond to the start of the steady-state water flow at  $\sigma = 0$  (saturated state,  $S = 1.0$  is assumed)

## 4 Experimental Results and Discussion

### 4.1 Oedometric Swelling Behavior

The results of the oedometric swelling tests are presented in the following. Specific values are given for discussion while the full results are given in Tables 6 and 11 in Appendix A. Therein, the swelling pressure  $\sigma_{max}$  at Point B ( $\epsilon = 0$ , see Fig. 9), the strain  $\epsilon$  at points C and  $\epsilon_{max}$  D for all tests and the swelling indices for multi-step tests are summarized.

#### 4.1.1 Path-Dependency: Influence of the Loading Sequence

The experimental results of all swelling tests are evaluated in terms of void ratio vs. stress.

The presented paths are depicted by arrows in a semi-logarithmic plot. Assuming that those paths follow the swelling law of Grob (1972)

$$\Delta\epsilon = -k \log_{10} \left( \frac{\sigma_0}{\sigma_{max}} \right), \tag{2}$$

wherein  $\sigma_0$  is the fixing stress,  $\sigma_{max}$  the swelling pressure and  $k$  the corresponding swelling index, or its modification

$$\Delta e = \begin{cases} -C_S \log_{10} \left( \frac{\sigma_0}{\sigma_{max}} \right) & \text{for unloading,} \\ -C_C \log_{10} \left( \frac{\sigma_0}{\sigma_{max}} \right) & \text{for loading,} \end{cases} \tag{3}$$

the pairs of stress and void ratio at each step of multi-step tests can be characterised by a unique line whose slope can be determined similarly to Eq. 1 such as the swelling index  $C_S$  (unloading) and compression index  $C_C$  (loading). The swelling indices are evaluated over the total stress

range of the respective tests (either unloading to point C ( $\sigma = 0.5 \cdot \sigma_{max}$ ), or to point D ( $\sigma = \sigma_{max}$ )). It has to be noted, that the results of the tests with full unloading may be more accurate as they include two stress levels.

As can be seen in Fig. 10a, the variation of the control variable during unloading does not influence the magnitude of the swelling index. Both indices of the two representative multi-step tests with stress controlled unloading  $C_{S,OPA-0-04} = 0.0515$  and  $C_{S,OPA-0-07} = 0.0516$  are in good agreement and only slightly smaller than of the test with strain controlled unloading  $C_{S,OPA-0-29} = 0.0653$ . Extrapolated to  $\sigma = \sigma_0$  this results in very similar values for void ratio or strain, which are noticeably smaller than for the single-step swelling strain test on specimen OPA-0-24. A possible influence of the increment of the unloading steps can be assessed in Fig. 10b by evaluating the test on specimen OPA-1-11 with a first unloading step to  $\sigma = 0.75 \cdot \sigma_{max}$ . Taking possible scatter of the tests into account, the swelling index is determined to  $C_{S,OPA-1-11} = 0.0376$ . The loading of specimens OPA-1-15 and 1-16 after free axial swelling is presented in Fig. 11. The compression indices  $C_{C,OPA-1-15} = 0.0801$  and  $C_{C,OPA-1-16} = 0.1078$  are approximately twice as large as the swelling indices  $C_S$  of the unloaded specimens.

Overall, a significant path-dependency of deformation is identified. The deformation and resulting void ratio during unloading from the swelling pressure are significantly smaller than during free axial swelling, where the deformation takes place driven by the initial saturation. An extrapolation of the loading path to the initial void ratio results in stress larger than the swelling pressure, which corresponds to the generally known distinction of stresses during swelling according to Sridharan et al. (1986).

The temporal evolution of stress and strain in the tests is shown in Figs. 12, 13 and 14. The tests that have already been discussed in detail are shown in saturated color, while

**Table 6** Results of the oedometric swelling tests

Specimen OPA-	B: $\sigma_{max}$ [MPa]	C: $\epsilon$ [%]	D: $\epsilon_{max}$ [%]	$C_S/C_C$ [-]
1-35	0.875	–	–	–
0-04	0.743	0.00715	0.05891	0.0515
0-07	0.663	0.00953	0.05144	0.0516
1-11	0.839	0.00251 <sup>1</sup>	0.04463 <sup>1</sup>	0.0376
0-29	0.958	0.01514 (C') <sup>2</sup>	0.02768 (C'') <sup>2</sup>	0.0653
0-24	–	–	0.09065	–
1-15	–	0.03052 <sup>3</sup>	0.09737	0.0801 <sup>5</sup>
1-16	0.01291 ( $\epsilon_{max}$ ) <sup>4</sup>	0.039	0.11271	0.1078 <sup>5</sup>

<sup>1</sup> Unloading to  $\sigma = 0.75 \cdot \sigma_{max}$

<sup>2</sup> Unloading to  $\epsilon \approx 0.20 \cdot \epsilon_{max}$  and  $\epsilon \approx 0.45 \cdot \epsilon_{max}$

<sup>3</sup> Loaded to an estimated stress of  $\sigma \approx 0.45 \cdot \sigma_{max}$

<sup>4</sup> Loaded to an estimated stress of  $\sigma \approx 0.90 \cdot \sigma_{max}$

<sup>5</sup> Compression index

**Fig. 10** Void ratio vs. stress for multi-step swelling tests. Unloading after single-step swelling stress test: **a** Stress vs. strain controlled unloading and **b** Stress controlled unloading with different magnitudes

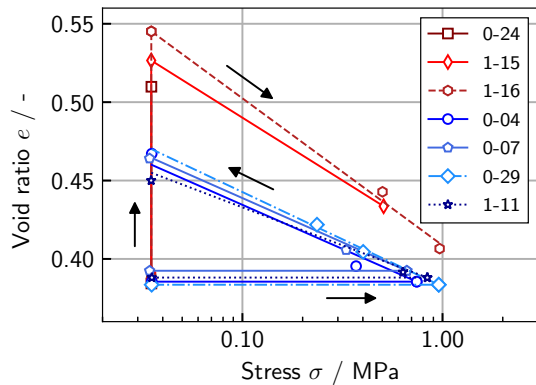
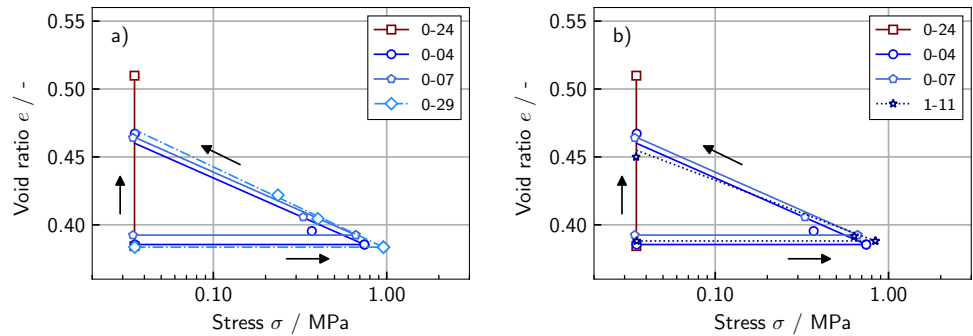
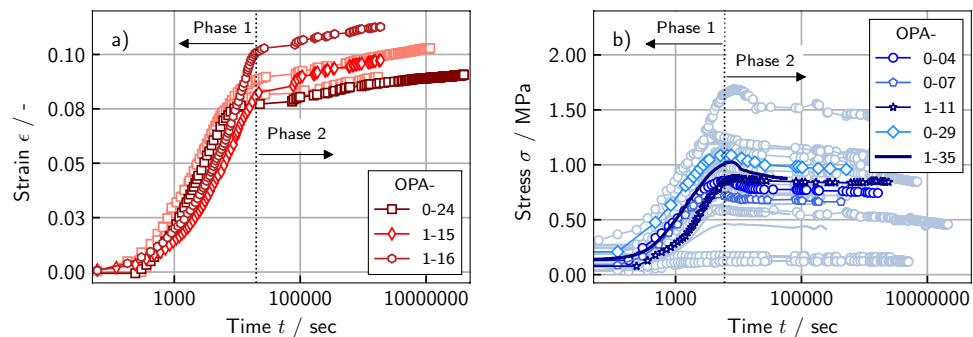


**Fig. 11** Void ratio vs. stress for multi-step swelling tests: loading after single-step swelling strain test

the remaining tests are shown in unsaturated color. Swelling tests conducted in *test setup 1* (manually controlled) are shown with markers while those conducted in *test setup 2* (servo-controlled) are shown with solid lines. For similar dry densities, a relatively large scattering can be noted. The results of single step tests demonstrate that the transient swelling behavior can be divided into two phases with different progressions for swelling under confined and unconfined conditions (Fig. 12). In multi-step testing it can be shown that the duration of each step can be significantly shorter when the sample is unloaded strain controlled instead of stress controlled. The temporal evolution of strain during unloading progresses more slowly than during the initial saturation.

**Fig. 12** Evolution of strain and stress during saturation in single-step tests: **a** Single-step swelling strain test (unconfined) and **b** Single-step swelling pressure test (confined)



### 4.1.2 Coupling Between Preloading Stress and Swelling Pressure

The swelling pressure increases with an increasing amount of expansive clay minerals per unit volume, hence with increasing dry density, cf. Villar and Lloret 2008; Zou et al. 2020; Middelhoff et al. 2019 and Schanz and Tripathy 2009, which also becomes evident in Fig. 12b. However, it is more convenient to correlate the compaction stress associated with the density, hence the preloading stress with the swelling pressure. Figure 15 shows the swelling pressure for different initial void ratios and the unique compression line from compaction. An affine trend line can be drawn for the results of all swelling pressure tests, which supports this approach.

### 4.1.3 Coupling Between Saturation and Swelling Behavior

A first phase with a pronounced evolution of swelling strain was observed for swelling under unconfined conditions (see Fig. 12a) followed by a second phase with a slower increase in strain. The question arises at what time the saturation had fully progressed through the entire specimen and if a coupling between saturation and deformation could be established and also be applied to swelling under confined conditions. These questions are addressed by testing two specimens in perspex rings. The progress of the saturation front is recorded during the measurement of strain/stress allowing a direct evaluation of the coupling

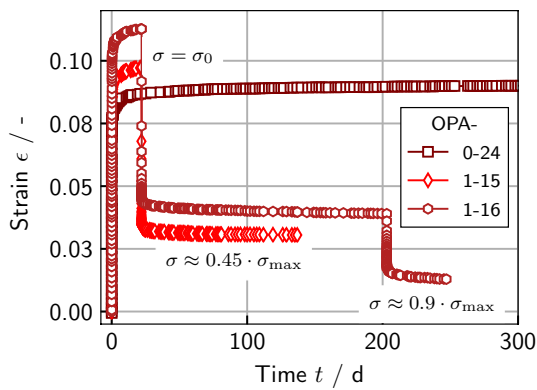


**Fig. 13** Evolution of strain during loading in multi-step swelling tests

between wetting and swelling. Pictures of a specimen in a perspex ring during saturation can be seen in Fig. 16. The results are displayed in Fig. 17 and summarised in Table 7.

The evolution of the axial strain and the saturation front of specimen OPA-0-15 under unconfined conditions proceeds parallel to each other and a linear coupling can be identified. The test has been stopped when the saturation front reached the top of the sample. The degree of saturation is determined to  $S = 0.98$ . The comparison of the maximum recorded strain  $\epsilon_{\max, \text{OPA-0-15}} = 0.0657$  to the strain of a single-step swelling strain test, e.g., OPA-0-24 (s. Fig. 12a), indicates that the saturation has approximately progressed through the entire specimen when the second phase is entered. The increase of strain in phase 1 is linear proportional to the degree of saturation or volumetric water content.

In the swelling pressure test on specimen OPA-0-14 the final degree of saturation was determined to  $S = 0.94$ . The stress relaxation in the second phase thus begins before full saturation is reached (s. Fig. 12b). The saturation front progresses more slowly than under confined conditions.

The linear coupling between saturation and deformation is confirmed by the results of the short swelling strain tests with variation of watering which are displayed in Fig. 18. Table 8 summarises the values for strain and degree of saturation at the end of both tests. It becomes evident that for the identical

**Fig. 14** Evolution of strain and stress during unloading in multi-step swelling tests: **a** stress controlled and **b** strain controlled

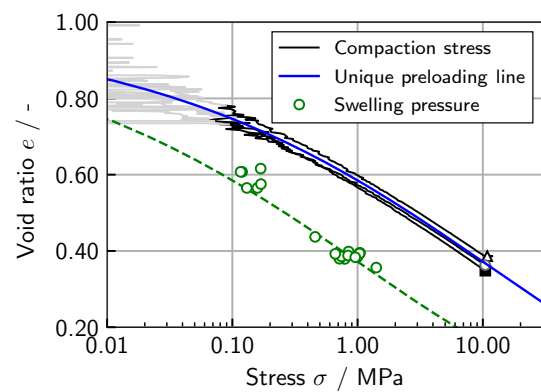
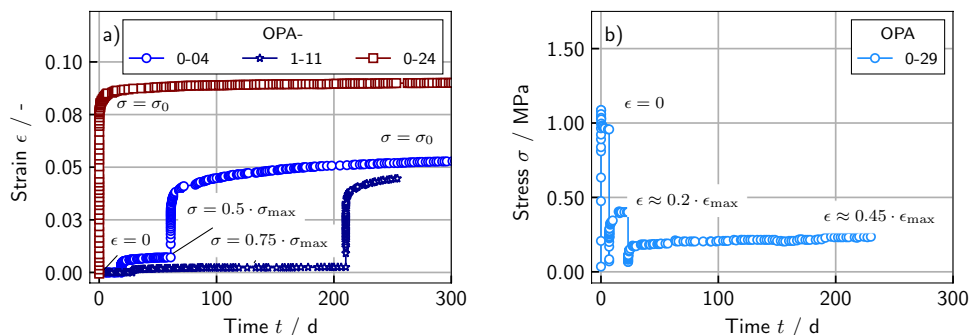


**Fig. 15** Results of swelling pressure tests with regard to the preloading state. Stress data from the load cell during compaction below its precision

time interval the watering from both sides results in a twice as large deformation and saturation of the specimen compared to the results from the test with watering from only one side. In agreement with the consolidation theory the same amount of deformation approximately takes four times as long for the twice as long drainage path.

### 4.2 Oedometric Compression Behavior Before and After Swelling Tests

Stress and deformation measurements during specimen preparation (Sect. 2.2) indicate a unique first compression line with the compression index  $C_{C, \text{prep}} = 0.208$ , which gives the preparation stress, hence preloading pressure, for a specific targeted void ratio, e.g.,  $\sigma_{v, \text{prep}} = 10.16$  MPa for  $e_0 = 0.430$  ( $\rho_d = 1.901$  g/cm<sup>3</sup>). The results of oedometric compression tests on nearly dry material before saturation support these findings. As it is shown in terms of void ratio vs. stress in Fig. 19a the magnitude of  $C_C$ ,  $C_S$  as well as the relation between  $\sigma_{\text{prep}}$  and  $\rho_d$  is confirmed. The mean value of the compression index obtained from oedometric testing  $\bar{C}_{C, \text{dry}} = 0.220$  is only slightly higher than during preparation. The swelling index was overestimated before and can now be determined more precisely to  $\bar{C}_{S, \text{dry}} = 0.015$ . The preloading

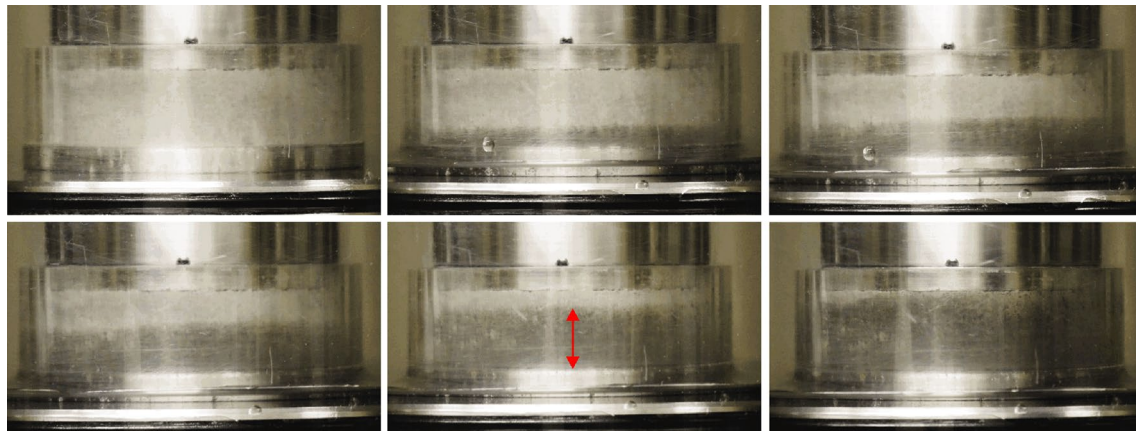


Fig. 16 View of specimen OPA-0-15 during different stages of a single-step swelling strain test in a perspex oedometer ring

stress, calculated from the intersection of the tangents of the first compression line and elastic unloading/reloading line, confirms the magnitude registered during preparation. All test results are well reproducible, even for high stress levels. A summary the results are presented in Table 9.

The results of swelling tests with subsequent oedometric compression tests are shown in Fig. 19b in terms of void ratio vs. stress. In contrast to the oedometric compression tests on dry material, these are not continuously recorded measured values, but only the values at the end of each loading step. The time–compression and time–decompression plots for all three tests are given in the Appendix B confirming drained conditions and completed consolidation at the end of the loading step.

Several observations can be made from the stress-void ratio plots: The first section of the loading path shows a similar slope as the un- and reloading paths, except for specimen OPA-0-24 (red plot in Fig. 19b) which is missing data in this section. The slope of the un- and reloading paths is significantly higher than in the oedometric compression tests on unsaturated specimens. A severe increase of the swelling index  $\bar{C}_s = 0.055$  and hence reduction of the un- and reloading stiffness is observed (factor 3.7). The later section of the loading path exhibits a similar slope  $\bar{C}_c = 0.174$  as the dry samples (factor 1.2), but shifted to an area of a notably smaller stress level, which indicates a noticeable reduction of preloading stress. For all three specimens tested after swelling an approximately unique compression line is identified for stresses larger than 1 MPa, independent of the type of the prior swelling test. A transitional area for smaller stresses can be determined with the prior swelling test influencing the mechanical response only in this stress range. For very large stresses a further reduction of stiffness seems to occur in the area of extremely small void ratios. It is assumed that the grain size distribution and microstructure

of the reconstituted specimens may be affected by these large stresses - i.e., resulting in pore collapse - and an evaluation in terms of void ratio is not suitable. The existence of a normal compression line (NCL), which is approximated by all specimens in the saturated state, can be concluded.

The magnitude of the compression and swelling indices observed in oedometric compression tests are compared to the results of the oedometric swelling tests, see Sect. 4.1. Figure 20 shows the unloading paths of selected oedometric swelling tests (black) and the oedometric compression tests in the saturated state (in color). Overall, a

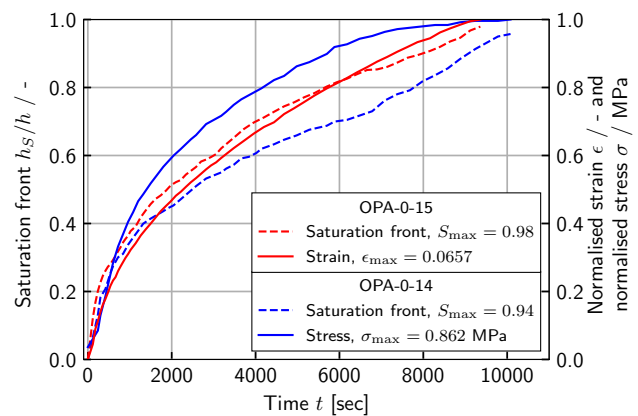
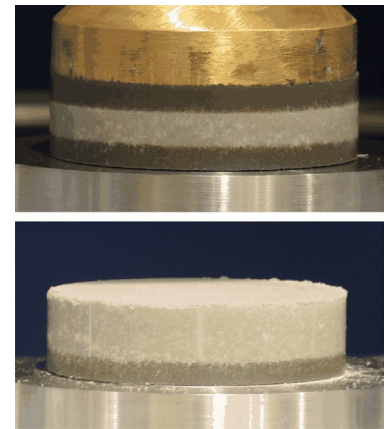
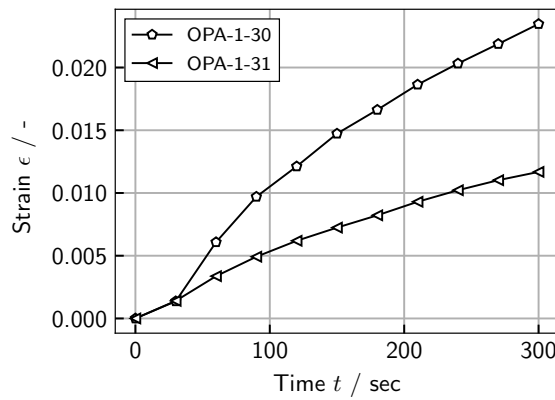


Fig. 17 Testing in perspex rings: Evolution of the saturation fronts, strain and stress. Strain and stress are normalised to their maximum values

Table 7 Results of the oedometric swelling tests in perspex rings

Specimen OPA-	Path	$\sigma$ [MPa]	$\epsilon$ [%]	$S$ [-]	$t$ [h:mm]
0-14	A-B	0.862	Const.	0.94	2:48
0-15	A-D	Const.	6.57	0.98	2:36

**Fig. 18** Initial phase of single-step swelling strain tests with variation of watering: Strain vs. time and view of the specimens after testing



**Table 8** Results of the short swelling strain tests with variation of watering

Specimen OPA-	Watering	$\epsilon$ [%]	$S$ [-]
1-30	Top, bottom	2.53	0.60
1-31	Bottom	1.13	0.29

reduced, but constant unloading and reloading stiffness can be derived in the saturated state, which is assumed to be independent of both, stress level and void ratio. The loading stiffness of the swelling tests can be evaluated as an elastic reloading stiffness in the transitional area before the NCL is reached.

The magnitude of the compression and swelling indices in the saturated state are in good accordance with those reported by Crisci et al. (2019) and Favero et al. (2016) for remoulded specimen. As expected, they differ from those of the intact shale, as the extremely small void ratios could not be achieved during compaction of the reconstituted specimens. For the behaviour in oedometric compression tests in the saturated state, the sample preparation method-remoulded as a slurry with a certain multiple of the liquid limit or dry compacted and then saturated-does not seem to have a significant influence. However, with remoulded specimens, the preloading history of the specimen is not known, so that the degradation of the material due to saturation and swelling cannot be assessed.

### 4.3 Permeability

The results of steady-state air permeability tests on the unsaturated specimens are presented in Table 10. According to Klinkenberg (1941) the flow of gas through porous media is pressure-dependent. For smaller pressures the slip-effect along the walls of the pore channels is more pronounced and a higher gas flow rate, thus higher permeability, can be observed. The so called *Klinkenberg effect* can be neglected for very large pressures and the gas-phase permeability becomes the true permeability  $K_\infty$  according to

$$K_a = K_\infty \left( 1 + \frac{b}{p} \right), \tag{4}$$

wherein  $K_a$  is the apparent permeability,  $b$  the Klinkenberg factor and  $p$  the applied air pressure. With an apparent unsaturated permeability  $K_a = K_{dry} = 1.45 \cdot 10^{-15} \text{ m}^2$  at a mean pressure of  $\bar{p} = 50 \text{ kPa}$  and an estimation for the Klinkenberg factor  $b = 47.5 \text{ kPa}$  (Wu et al. 1998) the true unsaturated permeability results to  $K_{dry,\infty} = 7.44 \cdot 10^{-16} \text{ m}^2$  for the non swollen material.

The evaluation of permeability from steady-state water permeability in the wet state is also presented in Table 10. A reduction of the permeability by three orders of magnitude can be observed for both samples OPA-0-22 (multi-step test) and OPA-0-35 (single step swelling strain test) from the

**Fig. 19** Void ratio vs. stress for all oedometric compression tests: **a** before saturation and **b** after saturation

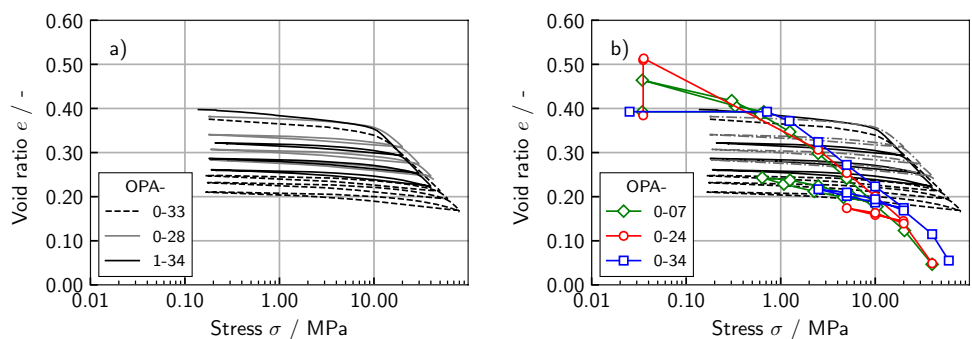


**Table 9** Oedometric compression tests before and after swelling: mechanical properties

Specimen OPA-	$C_c$ [-]	$C_s$ [-]	$\sigma_v$ [MPa]
1-34	0.226	0.018	9.6
0-33	0.215	0.014	11.6
0-28	0.218	0.012	12.1
0-07	0.179	0.058	-
0-24	0.163	0.053	-
0-34	0.180	0.054	-

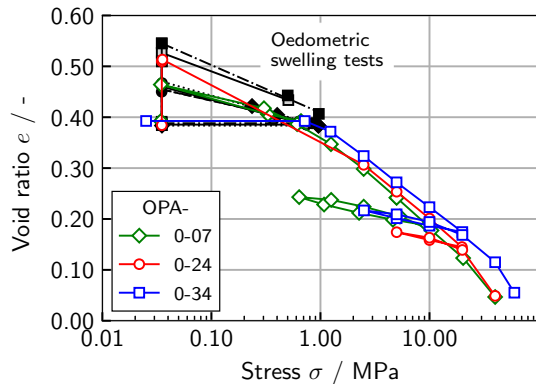


**Fig. 20** Void ratio vs. stress for oedometric compression tests after saturation and selected multi-step swelling tests

dry to the wet state. Under volume constant conditions the contributing porosity has been significantly reduced by the swelling process whilst the global volume, hence the porosity, remained constant in sample OPA-0-22. The subsequent unloading of the sample and the vertical deformation led to a minor increase of the permeability. The same observation is made for the more increased permeability in the saturated sample OPA-0-35. Analogously to the results of the oedometric swelling tests, see Sect. 4.1, the strain at the end of the single-step test is larger than after unloading.

In comparison to the magnitude of permeability in the dry state and taking into account the general uncertainties that occur during permeability testing (see i.e., Winhausen et al. 2021), a

**Table 10** Results of the performed permeability testing

Specimen OPA-	State	Fluid	$e$ [-]	$K$ [m <sup>2</sup> ]
0-08 – 0-13	Unsaturated	Nitrogen	0.389	$5.38 \cdot 10^{-16}$
0-22	Saturated, A	Water	0.387	$1.20 \cdot 10^{-18}$
	Saturated, D		0.387/0.460 <sup>1</sup>	$1.56 \cdot 10^{-18}$
0-35	Saturated, D	Water	0.387/0.502 <sup>2</sup>	$2.57 \cdot 10^{-18}$

<sup>1</sup> Multi-step test: after unloading from swelling pressure  $\epsilon = 5.3\%$

<sup>2</sup> Single-step swelling strain test  $\epsilon = 8.3\%$

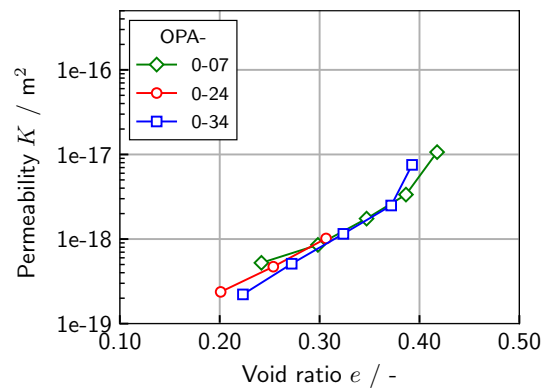


**Fig. 21** Evaluation of permeability [m<sup>2</sup>] from loading paths of oedometric compression tests in the saturated state

mean value of saturated permeability of  $K_{sat} = 1.78 \cdot 10^{-18} \text{ m}^2$  can be determined. Due to swelling the permeability of the material is thus reduced by a factor of approximately 300. For constant volume conditions the reduction the permeability even amounts to a factor of approximately 600.

The permeability  $K$  [m<sup>2</sup>] was further estimated during loading in the oedometric compression tests under saturated conditions. In Fig. 21 it is shown as a function of the void ratio at the beginning of each loading step. Following Casagrande’s log-time method the coefficient of consolidation  $c_v$  was evaluated from the time-settlement-curves (see Appendix B) and the permeability derived. For the three oedometric compression tests an almost unique relation can be established. The mechanical compaction and associated reduction of porosity, hence void ratio, strongly influence the permeability, which ranges between  $2.37 \cdot 10^{-19}$  and  $1.01 \cdot 10^{-17} \text{ m}^2$ . This observation is in good agreement with the results from swelling tests in perspex rings (see Sect. 4.1.3, where saturation was slower for smaller void ratios (volume constant swelling, lower permeability) than for larger void ratios (free axial swelling, higher permeability)). The estimated permeability from oedometric compression tests agrees well with that from the permeability tests.

#### 4.4 Summary

The results of the individual test methods correspond well and can be related with each other. Especially the tests in perspex rings provide new insights into the coupling of saturation and swelling phenomena and are in good accordance with the observed permeability trends. It becomes evident, that the time-dependent processes during swelling are closely linked to those during consolidation and can be attributed to diffusion. Overall, the test results show a close coupling of mechanical and hydraulic processes that influence both the temporal behaviour of a swellable material and its equilibrium states.

## 5 Interpretation of Experimental Results for Constitutive Modelling

The results of the experimental campaign partly served for the development of a novel constitutive model that was recently published by the authors in Grandas Tavera et al. (2022). Here, the observed phenomena from the experiments are discussed in regard to their significance concerning constitutive modelling in general.

Samples subjected to oedometric unloading after single-step swelling stress tests show a significantly smaller deformation in contrast to free swelling tests under the same stress conditions, see Figs. 10 and 11. Furthermore, the swelling index determined here and in the oedometric compression tests is significantly larger in the saturated state than in the dry state, see Fig. 19. It can be observed that the saturation of the sample leads to a degradation of the elastic stiffness. Therefore, the swelling index is not a constant but a function of the degree of saturation, i.e.,  $\kappa = \kappa(S)$  (or  $C_S = C_S(S)$ ) holds.

A division of the total strain into a swelling strain and an elastic (mechanical) strain—as proposed by Grob's swelling law (Grob 1972) and its implementation in several numerical frameworks, see Anagnostou 1993; Heidkamp 2004 or Wittke-Gattermann and Wittke 2004—seems not convenient, because both the swelling strain and the elastic strain depend on the degree of saturation.

Results from Nowamooz and Masrouri (2008), Monroy et al. (2015) and Hong et al. (2010) amongst others indicate that upon long oedometric compression up to several megapascals both dry and fully saturated samples approach an unique first loading line in the  $e - \log \sigma$ -space. For smaller stresses however dry and saturated samples followed different paths in the  $e - \log \sigma$ -space. In these cases, the first loading line for of saturated samples has the same slope but is shifted to the left when compared to the first loading line of dry samples (preloading line, PL) see Fig. 19. Instead of deriving an apparent dependency of  $\lambda$  (or  $C_c$ ) on suction or saturation from the latter observation, we describe these paths as transitions from overconsolidated (nearly reloading

paths) to normal consolidated states on the unique first loading line. This unique first loading line acts as an attractor because it is reached after long monotonic compression regardless of the saturation and the initial state. This means, that the loading history of the sample becomes less relevant when reaching this line because the preloading stress corresponds to the current one (normal consolidation).

For a given material, this line, the so called Normal Compression Line (NCL) (Nowamooz and Masrouri 2008) has a fixed position and constant slope. For a consistent description of the material behaviour, the slope  $\lambda$  (or  $C_c$ ) of NCL must be independent of suction or saturation.

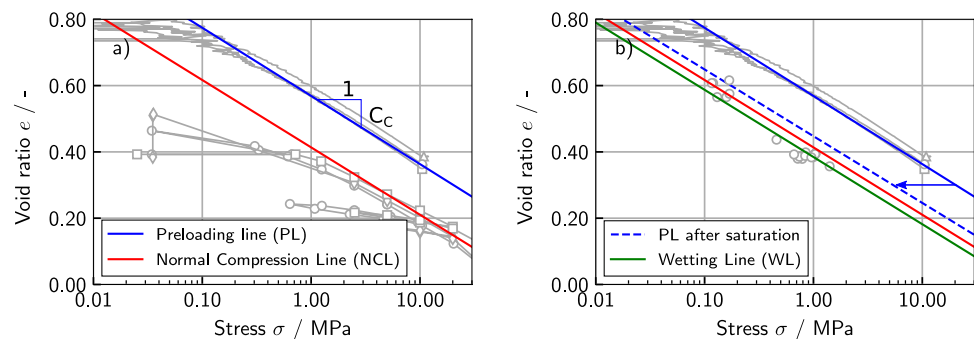
As an interim conclusion, it is emphasised that saturation degrades the preloading state and the elastic behaviour. For the partially saturated state, a large part of the material behaviour can already be interpreted and represented constitutively in this way. However, it is not yet sufficient for the description of expansive materials and the corresponding swelling phenomena.

In addition to the affinity of the PL in the dry state and the NCL, Fig. 15 suggests a further affinity between the PL and a line connecting the equilibrium swelling pressures for different void ratios, introduced as the wetting line (WL). In these tests, the preloading line corresponds also to a line connecting the preloading states for each swelling experiment before saturation.

The three derived lines and the corresponding experimental data (here only hinted in gray) are shown in Fig. 22a and b. Note that the WL is assumed to be left to the NCL in this presentation always since the NCL acts as an attractor for subsequent loading paths. The PL is shown in its initial state and in the saturated state, taking the reduction of preloading pressure into account.

Figures 15 and 22b also show that the swelling pressure decreases for smaller initial preloading stresses. As already indicated in Sect. 4.1.2, the magnitude of swelling pressure—at least for bentonite—is often correlated with the (dry) density (Villar and Lloret 2008; Zou et al. 2020; Middelhoff et al. 2019; Schanz and Tripathy 2009). However, the correlation between swelling pressure and preloading stress seems much

**Fig. 22** Interpretation of experimental data regarding the three characteristic lines. PL (derived from specimen preparation) is shown together with **a** NCL (derived from oedometric compression tests in the saturated state) and **b** WL (based on equilibrium swelling pressures)





more suitable, since the significance of preloading on the mechanical behavior has already been established. A higher preloading stress level does not only result in a larger amount of expansive clay minerals to be present per volume unit, but also into a more compact arrangement of the particles—both leading to larger swelling pressures and swelling deformations.

However, from the constitutive point of view, an additional mechanism is necessary for the material to swell. As shown by the results of testing in perspex rings in Sect. 4.1.3, swelling is directly coupled to the saturation process for both confined and unconfined conditions. The logical consequence is to introduce one and the same hydro-mechanically coupled process for the development of both swelling phenomena depending on the degree of saturation, a swelling mechanism. By interpreting this as an internal swelling strain  $\epsilon^w = \epsilon^w(S)$ , the respective phenomenon—i.e., expansion or swelling pressure—automatically results from the mechanical boundary condition as it also occurs in the laboratory. Note that this internal swelling strain needs to be fully integrated in the coupled system, more details can be found in Grandas Tavera et al. (2022). Common approaches introduce the degree of saturation to hydro-mechanically coupled constitutive models by, e.g., making the compression index a function of the degree of saturation (see Zhou et al. 2012; Bosch et al. 2021). Any change in degree of saturation then demands either changes in stress or strain depending on the boundary conditions. However, to the authors' knowledge, the here proposed direct proportionality between a wetting-induced strain and a change in the degree of saturation has not been presented in the literature.

In this way the final states of oedometric swelling tests and oedometric compression tests can be well described. The time evolution of deformation or stress during the tests though is strongly dependent on the hydraulic properties of the system, hence the permeability. It is well known that the permeability decreases due to swelling, but to the authors' knowledge, a quantitative assessment of the reduction has hardly been carried out. The results of permeability testing in this study including reference measurements in the unswollen state, see Sect. 4.3, show that the reduction is more severe for confined conditions, hence swelling pressure tests, as for unconfined conditions. This is due to the fact that expansion into the pore space takes place and for volume constant conditions the total available volume is limited. The lower permeability in the saturated state compared to the unsaturated state also manifests itself in the fact that the development of swelling strain takes considerably more time during unloading than during the initial saturation. Overall a mass transfer from mobile to immobile water takes place in the material during swelling processes yielding a reduction in effective pore space. This reduction varies with the boundary conditions and can be accounted for by introducing a separate water phase into the coupled system.

## 6 Conclusion

The material behavior of reconstituted Opalinus clay shale from Mont Terri, Switzerland, was studied experimentally under dry and drained conditions. The main objective of this study was to assess the hydro-mechanically coupled processes in a swellable clay shale and to derive fundamental characteristics for the continuum mechanical description of the material. Special attention was paid to linking the results of individual experimental methods. A consistent procedure for specimen preparation and several testing methods were presented together with the discussion and interpretation of the results. The following conclusions can be drawn with regard to the hydro-mechanically coupled material behaviour of reconstituted Opalinus Clay shale:

1. The material behavior during specimen preparation and whilst subjected to monotonic loading is characterised by a unique preloading line (PL) in the dry state. For each dry density or void ratio, a corresponding preloading stress was identified, which is decisive for the further material behavior.
2. In the saturated state, a parallel shift of the PL to areas of smaller stresses indicated a significant reduction of preloading stress. The slope of the first compression line remained unaffected by the degree of saturation. In contrast, the elastic stiffness of the material was severely reduced in the saturated state and can be described as a function of the degree of saturation.
3. Saturated compression converged to a unique line or normal compression line (NCL) regardless of the mechanical boundary conditions during saturation and loading path.
4. Equilibrium swelling pressure and swelling strain were always to the left of the PL and the NCL. An affine trend line was identified for the results of all swelling pressure tests indicating a correlation between preloading stress and swelling behavior, introduced as the wetting line (WL). Thus, the development of swelling strain/pressures depends on the preconsolidation stress and, reciprocally, the preloading stress evolves during swelling.
5. Samples with the same initial state but subjected to different loading paths (unconfined and confined swelling followed by unloading, respectively) developed different strains which indicates a significant path dependency.
6. A linear coupling between volumetric deformation and initial water propagation became evident for wetting under unconfined boundary conditions. For confined conditions, swelling pressure also developed as a result of the wetting, but saturation progressed more slowly due to a lower permeability. From a phenomenological

point of view, one single swelling mechanism induces either strain or stress depending on the global boundary conditions.

7. A swelling induced reduction of permeability in the saturated state was found with a factor of up to 600 for volume constant conditions. The influence of the mechanical boundary conditions on the permeability can be correlated with the void ratio.

This extensive experimental campaign on Opalinus Clay shale allows an assessment of the hydro mechanically coupled processes in the material. Observations from individual experimental methods could be confirmed by using experimental results derived through other methods. It was shown that the results of this study are in good accordance with previous studies on remoulded and reconstituted Opalinus Clay shale. Therefore, for the use of reconstituted clay shales in the engineered barrier system, the obtained results can

directly be applied. For the material behavior of the intact clay shale, further studies on the anisotropy of swelling and other consequences of diagenesis are required. However, previous studies suggest that, phenomenologically, the reduction of porosity alone due to the high preloading has a mayor influence on, e.g., the stiffness (see Favero et al. 2016). This allows at least a partial extrapolation of the presented results to intact materials. Overall, valuable knowledge regarding stress and strain development due to hydraulic and mechanical loading paths was gathered and their significance regarding constitutive modelling was presented.

## Appendix A: Results of All Oedometric Swelling Tests

See Appendix Table 11

**Table 11** Results of the oedometric swelling tests

Specimen OPA-	B: $\sigma_{\max}$	C: $\epsilon$ [%]	D: $\epsilon_{\max}$ [%]	$C_S/C_C$ [-]
1-01	0.458	–	–	–
1-02	1.409	–	–	–
1-03	0.847	–	–	–
1-09	0.130	–	–	–
1-12	1.037	–	–	–
1-21	0.169	–	–	–
1-22	0.168	–	–	–
1-04	1.047	0.00602	–	0.0283
1-05	1.032	0.00751	–	0.035
1-07	0.120	0.0045	–	0.0241
0-03	0.861	0.0091	–	0.0419
0-05	0.789	0.00753	–	0.0345
0-04	0.743	0.00715	0.05891	0.0515
0-02	0.713	0.00844	0.04364	0.0436
0-06	0.718	0.00849	0.04662	0.0455
0-07	0.663	0.00953	0.05144	0.0516
1-06	0.997	0.00741	0.05029	0.0429
1-08	0.116	0.00399	0.00538	0.016
1-10	0.159	0.00574	0.01083	0.0263
1-11	0.839	0.00251 <sup>1</sup>	0.04463 <sup>1</sup>	0.0376
0-29	0.958	0.01514 (C'') <sup>2</sup>	0.02768 (C'') <sup>2</sup>	0.0653
0-24	–	–	0.09065	–
0-32	–	–	0.0899	–
1-17	–	–	0.10293	–
1-15	–	0.03052 <sup>3</sup>	0.09737	0.0801 <sup>5</sup>
1-16	0.01291 ( $\epsilon_{\max}$ ) <sup>4</sup>	0.039	0.11271	0.1078 <sup>5</sup>

<sup>1</sup> Unloading to  $\sigma = 0.75 \cdot \sigma_{\max}$

<sup>2</sup> Unloading to  $\epsilon \approx 0.20 \cdot \epsilon_{\max}$  and  $\epsilon \approx 0.45 \cdot \epsilon_{\max}$

<sup>3</sup> Loaded to an estimated stress of  $\sigma \approx 0.45 \cdot \sigma_{\max}$

<sup>4</sup> Loaded to an estimated stress of  $\sigma \approx 0.90 \cdot \sigma_{\max}$

<sup>5</sup> Compression index

### Appendix B: Oedometric Compression Tests in the Saturated State: Time-Compression and Time-Decompression Plots

See Appendix Figs. 23, 24, 25.

**Fig. 23** Time-(de)compression curves for specimen OPA-0-07: loading, unloading, reloading

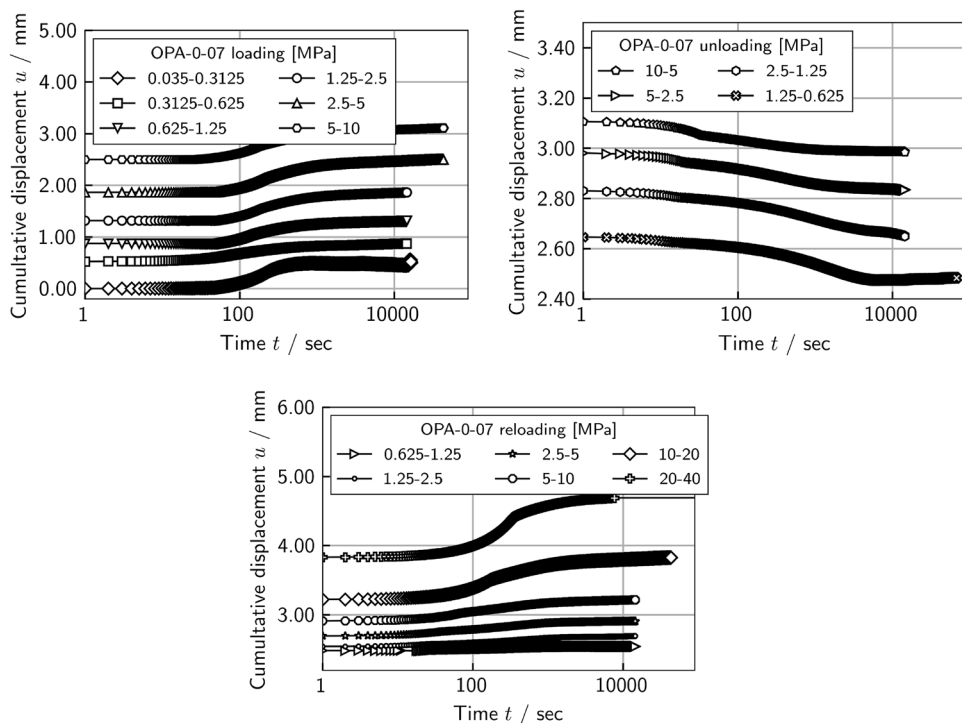


**Fig. 24** Time-(de)compression curves for specimen OPA-0-24: loading, unloading, reloading

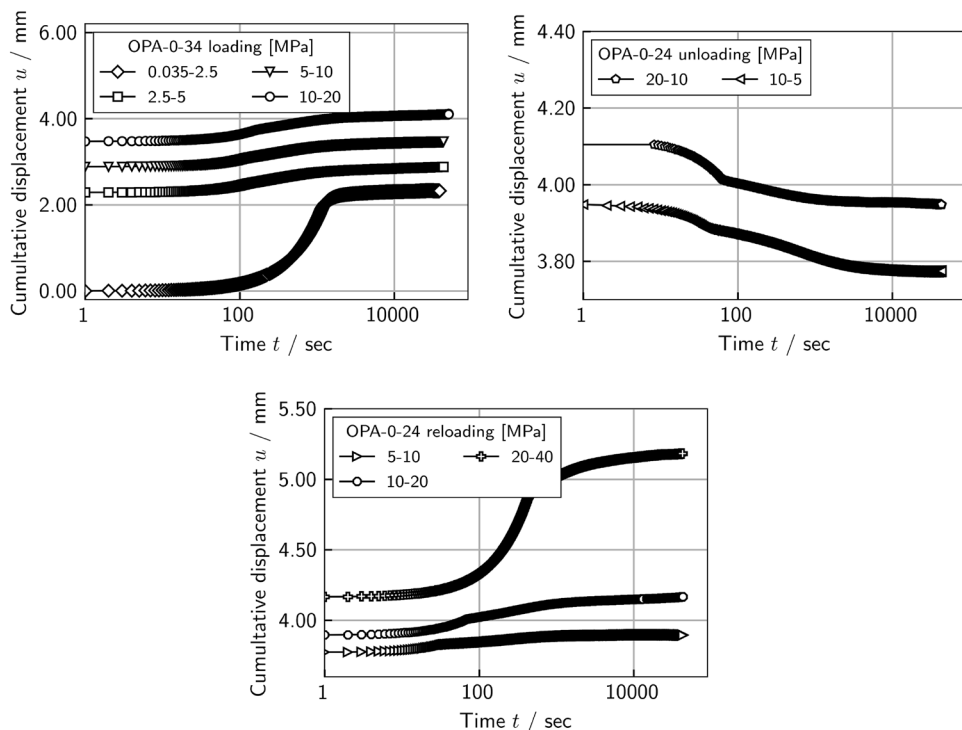
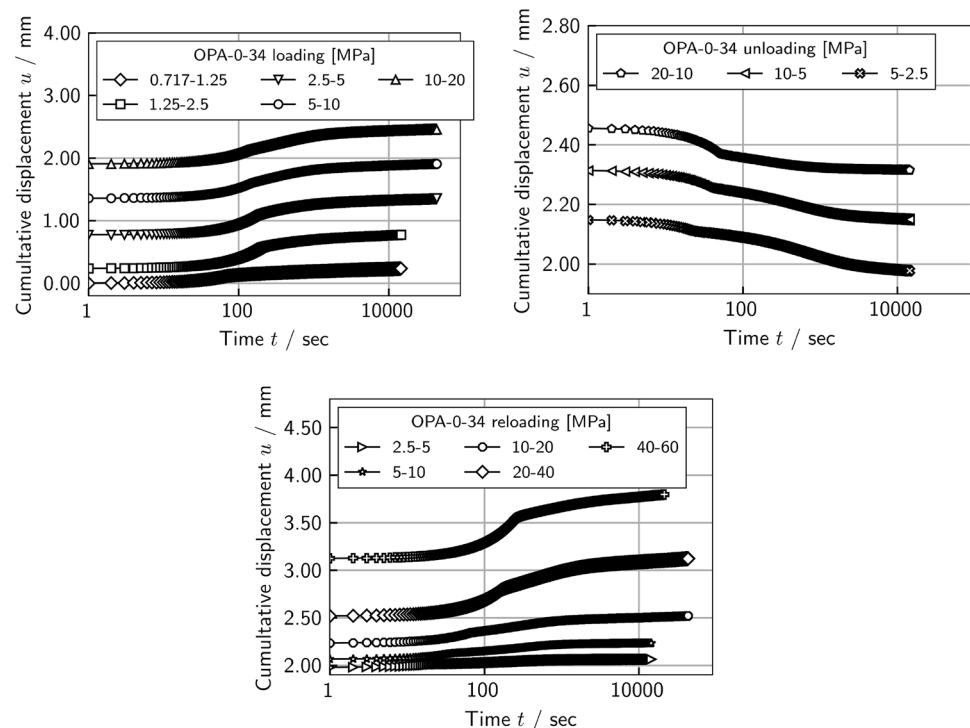


**Fig. 25** Time-(de)compression curves for specimen OPA-0-34: loading, unloading, reloading



**Acknowledgements** The authors would like to thank swisstopo and the Mont Terri Underground Rock Laboratory for supplying the material. The department of Geochemistry & Economic Geology and Engineering Geology at the Institute of Applied Geosciences at Karlsruhe Institute of Technology for the analysis of the mineralogical composition of the material and assistance with specimen preparation. Special thanks to the laboratory staff of the Institute of Soil Mechanics and Rock Mechanics at Karlsruhe Institute of Technology for the help during the realisation of the experimental campaign.

**Funding** Open Access funding enabled and organized by Projekt DEAL. No funding was received for conducting this study.

## Declarations

**Conflict of interest** All experimental data can be shared on request.

**Open Access** This article is licensed under a Creative Commons Attribution 4.0 International License, which permits use, sharing, adaptation, distribution and reproduction in any medium or format, as long as you give appropriate credit to the original author(s) and the source, provide a link to the Creative Commons licence, and indicate if changes were made. The images or other third party material in this article are included in the article's Creative Commons licence, unless indicated otherwise in a credit line to the material. If material is not included in the article's Creative Commons licence and your intended use is not permitted by statutory regulation or exceeds the permitted use, you will need to obtain permission directly from the copyright holder. To view a copy of this licence, visit <http://creativecommons.org/licenses/by/4.0/>.

## References

Alonso EE, Gens A, Josa A (1990) A constitutive model for partially saturated soils. *Géotechnique* 40(3):405–430. <https://doi.org/10.1680/geot.1990.40.3.405>

Alonso EE, Vaunat J, Gens A (1999) Modelling the mechanical behaviour of expansive clays. *Eng Geol* 54(1):173–183. [https://doi.org/10.1016/S0013-7952\(99\)00079-4](https://doi.org/10.1016/S0013-7952(99)00079-4)

Anagnostou G (1993) A model for swelling rock in tunnelling. *Rock Mech Rock Eng* 26(4):307–331

Bosch JA, Ferrari A, Laloui L (2021) Coupled hydro-mechanical analysis of compacted bentonite behaviour during hydration. *Computers Geotech* 140:104447. <https://doi.org/10.1016/j.compgeo.2021.104447>

Bossart P (2012) Characteristics of the Opalinus clay at Mont Terri. Mont Terri Project, Wabern Switzerland

Chevalier G, Diamond LW, Leu W (2010) Potential for deep geological sequestration of CO<sub>2</sub> in Switzerland: a first appraisal. *Swiss J Geosci* 103(3):427–455

Crisci E, Ferrari A, Giger SB, Laloui L (2019) Hydro-mechanical behaviour of shallow opalinus clay shale. *Eng Geol* 251:214–227. <https://doi.org/10.1016/j.enggeo.2019.01.016>

Cui Y, Delage P (1996) Yielding and plastic behaviour of an unsaturated compacted silt. *Geotechnique* 46:291–311. <https://doi.org/10.1680/geot.1996.46.2.291>

Della Vecchia G, Dieudonné A-C, Jommi C, Charlier R (2015) Accounting for evolving pore size distribution in water retention models for compacted clays. *Int J Numerical Anal Methods Geomech* 39(7):702–723. <https://doi.org/10.1002/nag.2326>

Dieudonné A-C, Della Vecchia G, Charlier R (2017) Water retention model for compacted bentonites. *Can Geotech J* 54(7):915–925. <https://doi.org/10.1139/cgj-2016-0297>

Favero V, Ferrari A, Laloui L (2016) On the hydro-mechanical behaviour of remoulded and natural opalinus clay shale. *Eng Geol*. <https://doi.org/10.1016/j.enggeo.2016.04.030>

Ferrari A, Favero V, Laloui L (2016) One-dimensional compression and consolidation of shales. *Int J Rock Mech Mining Sci* 88:15–286300. <https://doi.org/10.1016/j.ijrmmms.2016.07.030>

Gens A, Alonso EE (1992) A framework for the behaviour of unsaturated expansive clays. *Can Geotech J* 29(6):1013–1032. <https://doi.org/10.1139/t92-120>

- Grandas Tavera C, Nitsch A, Machaček J (2022) A 1d hypoplastic constitutive model for expansive soils. *Acta Geotechnica*. <https://doi.org/10.1007/s11440-022-01548-y>
- Grob H (1972) Schwellendruck im Belchentunnel. In: *Proc Int Symp Für Untertagebau, Luzern*, pp. 99–119
- Heidkamp H, Katz C (2004) The swelling phenomenon of soils-Proposal of an efficient continuum modelling approach. *EUROROCK 2004 and 53rd Geomechanics Colloquium*
- Hong Z-S, Yin J, Cui Y-J (2010) Compression behaviour of reconstituted soils at high initial water contents. *Géotechnique* 60(9):691–700. <https://doi.org/10.1680/geot.09.P.059>
- Kiehl J (1990) Ein dreidimensionales quellgesetz und seine anwendung auf den felshohlraumbau. In: *Sonderheft der Zeitschrift Geotechnik, Vorträge zum 9. Nationalen Felsmechanik Symposium*
- Klinkenberg LJ (1941) The permeability of porous media to liquids and gases. In: *Drilling and Production Practice*. American Petroleum Institute
- Leuthold J, Gerolymatou E, Vergara M, Triantafyllidis T (2021) Effect of compaction banding on the hydraulic properties of porous rock: Part I-experimental investigation. *Rock Mech Rock Eng*. <https://doi.org/10.1007/s00603-021-02427-w>
- Lo K, Lee Y (2011) Time-dependent deformation behaviour of queenston shale. *Canadian Geotech J* 27:461–471. <https://doi.org/10.1139/t90-061>
- Marschall P, Horseman S, Gimmi T (2005) Characterisation of gas transport properties of the opalinus clay, a potential host rock formation for radioactive waste disposal. *Oil & Gas Sci Technol* 60(1):121–139
- Mašín D, Khalili N (2008) A hypoplastic model for mechanical response of unsaturated soils. *Int J Numer Anal Meth Geomech* 32(15):1903–1926. <https://doi.org/10.1002/nag.714>
- Mazurek M, Hurford AJ, Leu W (2006) Unravelling the multi-stage burial history of the swiss molasse basin: integration of apatite fission track, vitrinite reflectance and biomarker isomerisation analysis. *Basin Res* 18(1):27–50. <https://doi.org/10.1111/j.1365-2117.2006.00286.x>
- Middelhoff M, Cuisinier O, Masroufi F, Talandier J, Conil N (2019) Combined impact of selected material properties and environmental conditions on the swelling pressure of compacted claystone/bentonite mixtures. *Appl Clay Sci*. <https://doi.org/10.1016/j.clay.2019.105389>
- Mohajerani M, Delage P, Monfared M, Tang A-M, Sulem J, Gattmiri B (2011) Oedometric compression and swelling behaviour of the callovo-oxfordia, argillite. *Int J Rock Mech Mining Sci* 48:606–615. <https://doi.org/10.1016/j.ijrmmms.2011.02.016>
- Monroy R, Zdravkovic L, Ridley AM (2015) Mechanical behaviour of unsaturated expansive clay under k0 conditions. *Eng Geol* 197:112–131. <https://doi.org/10.1016/j.enggeo.2015.08.006>
- Nagra (2005) Darstellung und Beurteilung der aus sicherheitstechnisch-geologischer Sicht möglichen Wirtgesteine und Gebiete. Technical report
- Nagra (2014) Etappe 2: Vorschlag weiter zu untersuchender geologischer Standortgebiete mit zugehörigen Standortarealen für die Oberflächenanlage. Geologische Grundlagen. Nagra Wettingen, Switzerland. Nationale Genossenschaft für die Lagerung radioaktiver Abfälle
- Nowamooz H, Masroufi F (2008) Hydromechanical behaviour of an expansive bentonite/silt mixture in cyclic suction-controlled drying and wetting tests. *Eng Geo* 101:154–164. <https://doi.org/10.1016/j.enggeo.2008.04.011>
- Nygård R, Gutierrez M, Gautam R, Høeg K (2004) Compaction behavior of argillaceous sediments as function of diagenesis. *Marine Petrol Geol* 21(3):349–362. <https://doi.org/10.1016/j.marpetgeo.2004.01.002>
- Savage WZ, Braddock WA (1991) A model for hydrostatic consolidation of pierre shale. *Int J Rock Mech Mining Sci Geomech Abstracts* 28(5):345–354. [https://doi.org/10.1016/0148-9062\(91\)90073-U](https://doi.org/10.1016/0148-9062(91)90073-U)
- Schanz T, Tripathy S (2009) Swelling pressure of a divalent-rich bentonite: diffuse double-layer theory revisited. *Water Resour Res*. <https://doi.org/10.1029/2007WR006495>
- Seiphoori A, Whittle AJ, Krakowiak KJ et al (2017) Insights into diagenesis and pore structure of opalinus shale through comparative studies of natural and reconstituted materials. *Clays Clay Miner* 65:135–153. <https://doi.org/10.1346/CCMN.2017.064055>
- Seiphoori A, Moradian Z, Einstein HH, Whittle AJ (2016) Microstructural characterization of opalinus shale. 4:2742–2750
- Souza RFC, Pejón OJ (2020) Pore size distribution and swelling behavior of compacted bentonite/claystone and bentonite/sand mixtures. *Eng Geol*. <https://doi.org/10.1016/j.enggeo.2020.105738>
- Sridharan A, Rao A, Sivapullaiah P (1986) Swelling pressure of clays. *Geotech Testing J* 9(1):24–33
- Tang C-S, Tang A-M, Cui Y, Delage P, Shi B (2010) The coupled hydromechanical behaviour of compacted crushed callovo-oxfordian argillite. *J Rock Mech Geotech Eng* 2:86–90
- van Genuchten MT (1980) A closed-form equation for predicting the hydraulic conductivity of unsaturated soils. *Soil Sci Soc Am J* 44(5):892–898
- Vergara M (2019) Experimental and numerical investigations on the swelling behavior of claystone and sulfate rock. PhD thesis
- Vergara M, Balthasar K, Triantafyllidis T (2014) Comparison of experimental results in a testing device for swelling rocks. *Int J Rock Mech Mining Sci* 66:177–180
- Villar MV, Lloret A (2008) Influence of dry density and water content on the swelling of a compacted bentonite. *Appl Clay Sci* 39(1):38–49. <https://doi.org/10.1016/j.clay.2007.04.007>
- Wetzel A, Allia V (2003) Der Opalinuston in der Nordschweiz: Lithologie und Ablagerungsgeschichte. *Ecologiae Geologicae Helveticae* 96:451–469
- William E, Airey D (2009) The role of fabric in evaluating the failure mode of the stiffened bringelly shale. In: *Geological Society of London, UK (ed.) 10th IAEG International Congress IAEG 2006*
- Winhausen L, Amann-Hildenbrand A, Fink R, Jalali M, Khaledi K, Hamdi P, Urai JL, Schmatz J, Amann F (2021) A comparative study on methods for determining the hydraulic properties of a clay shale. *Geophys J Int* 224(3):1523–1539. <https://doi.org/10.1093/gji/ggaa532>
- Wittke-Gattermann P, Wittke M (2004) Computation of strains and pressures for tunnels in swelling rocks. *Tunn Undergr Space Technol* 19(4–5):422–423
- Wong RCK (1998) Swelling and softening behaviour of la biche shale. *Can Geotech J* 35(2):206–221
- Wu Y-S, Pruess K, Persoff P (1998) Gas flow in porous media with klinkenberg effects. *Transp Porous Media* 32(1):117–137. <https://doi.org/10.1023/A:1006535211684>
- Zeng Z, Cui Y-J, Talandier J (2021) Compaction and sealing properties of bentonite/claystone mixture: impacts of bentonite fraction, water content and dry density. *Eng Geol*. <https://doi.org/10.1016/j.enggeo.2021.106122>
- Zhang C-L, Kröhn K-P (2019) Sealing behaviour of crushed claystone-bentonite mixtures. *Geomech Energy Env* 17:90–105. <https://doi.org/10.1016/j.gete.2018.09.004>
- Zhang C, Rothfuchs T (2004) Experimental study of the hydro-mechanical behaviour of the callovo-oxfordian argillite. *Appl Clay Sci* 26(1):325–336. <https://doi.org/10.1016/j.clay.2003.12.025>

- Zhou A-N, Sheng D, Sloan SW, Gens A (2012) Interpretation of unsaturated soil behaviour in the stress-saturation space, I: volume change and water retention behaviour. *Computers Geotech* 43:178–187. <https://doi.org/10.1016/j.compgeo.2012.04.010>
- Zhou A-N, Sheng D, Sloan SW, Gens A (2012) Interpretation of unsaturated soil behaviour in the stress-saturation space: II: constitutive relationships and validations. *Computers Geotech* 43:111–123. <https://doi.org/10.1016/j.compgeo.2012.02.009>
- Zou W-l, Han Z, Ye J-b (2020) Influence of external stress and initial density on the volumetric behavior of an expansive clay during wetting. *Env Earth Sci* 79(10):211. <https://doi.org/10.1007/s12665-020-08960-1>

**Publisher's Note** Springer Nature remains neutral with regard to jurisdictional claims in published maps and institutional affiliations.